Published by SET Publisher

Journal of Basic & Applied Sciences

ISSN (online): 1927-5129

Hypersonic Boundary Layer Flow Over a Flat Plate with Applied Magnetic Field and Vectored Surface Mass Transfer

Mahesh Kumari[1] and Rama Subba Reddy Gorla[2,*]

[1]*Retired, Department of Mathematics, Indian Institute of Science, Bangalore - 560 012, India*

[2]*Department of Aeronautics and Astronautics, Air Force Institute of Technology, Wright Patterson Air Force Base, Dayton, Ohio 45433 USA*

Article Info:

Keywords:
Hypersonic,
Magnetic field,
Boundary layer,
Compressible flow,
Vectored surface mass transfer.

Timeline:
Received: March 01, 2025
Accepted: March 24, 2025
Published: April 26, 2025

Citation: Kumari M, Gorla RSR. Hypersonic Boundary Layer Flow Over a Flat Plate with Applied Magnetic Field and Vectored Surface Mass Transfer. J Basic Appl Sci 2025; 21: 119-127.

DOI: https://doi.org/10.29169/1927-5129.2025.21.12

Abstract:

A boundary layer analysis is presented for hypersonic flow over isothermal and adiabatic flat plates. Consideration is given to variable properties of air. It has been shown that surface drag and heat transfer rates can be controlled by applying magnetic field and vectored surface mass transfer. The range of Mach numbers considered is 2.5 to 10. As the magnetic field strength M increases, friction factor and heat transfer rate (for an isothermal surface) or surface temperature (for an adiabatic surface) increase. Friction factor and surface temperature (in the case of adiabatic surface) can be reduced by applying vectored surface mass transfer.

*Corresponding Author
E-mail: Rama.Gorla@afit.edu

1. INTRODUCTION

Aerodynamic heating is the heating of a surface due to flow of air at high speed. The kinetic energy of the air will be converted to thermal energy within the boundary layer. Prediction of the heat transfer rate to the surface at high Mach number flows is crucial to the design of thermal protection system. Tauber and Mennes [1] made engineering estimates of the aerodynamic heating to an aerospace plane. According to their estimates, aerodynamic heating during ascent (about $650\ W/cm^2$) dominates the design of the vehicle.

Klopfer and Yee [2] investigated viscous hypersonic flow on a blunt body. Hoffmann *et al*. [3] discussed the difficulties in predicting heat transfer rates for high speed flows. Qu *et al*. [4] presented an analysis for hypersonic heating. All these studies assumed a constant value of specific heat of air. Zhang *et al*. [5] provided a turbulence model for aerothermal prediction. Liu and Cao [6] studied the heat transfer in hypersonic boundary layer over a flat plate by taking into account of variable properties.

The present work is undertaken in order to study the effect of applied magnetic field and vectored surface mass transfer in the case of hypersonic flow over a flat plate. The properties of air are assumed to be temperature-dependent. Consideration is given to the application of transverse magnetic field in high speed aerodynamics where the air is ionized and changing the velocity and temperature fields as well as the drag and surface heat transfer rates. The application of a magnetic field enables control and potential reduction of drag and surface heat transfer. Such a mechanism is of extreme importance for flow over hypersonic vehicles. Rossow [7] was the first one to analyze the effect of magnetic field in the case of incompressible boundary layer flow. The use of vectored surface mass transfer is another mechanism to reduce surface heat transfer rate and finds application in boundary layer control on aerodynamic vehicles, film and transpiration cooling of rocket engines, turbomachinery blades etc. Gorla [8] studied the effect of vectored surface mass transfer in plane wall jet flows.

2. GOVERNING EQUATIONS

We consider the laminar, hypersonic boundary layer flow of an electrically conducting viscous fluid over a flat plate. An applied magnetic field B_0 is imposed on the boundary layer. We assume that the external flow is homentropic. We will consider both isothermal and adiabatic boundary conditions for the plate. We consider variable properties and include vectored surface mass transfer. The governing boundary layer equations may be written as:

$$\frac{\partial}{\partial x}(\rho u)+\frac{\partial}{\partial y}(\rho v)=0 \tag{1}$$

$$\rho u\frac{\partial u}{\partial x}+\rho v\frac{\partial u}{\partial y}=\frac{\partial}{\partial y}\left(\mu\frac{\partial u}{\partial y}\right)-{B_0}^2(\sigma u-\sigma_e u_e) \tag{2}$$

$$\rho C_P\left(u\frac{\partial T}{\partial x}+v\frac{\partial T}{\partial y}\right)=\frac{\partial}{\partial y}\left(k\frac{\partial T}{\partial y}\right)+\mu\left(\frac{\partial u}{\partial y}\right)^2 \tag{3}$$

The boundary conditions are given by

$$y=0: u=u_w,\ \ v=v_w,\ \ T = T_w(isothermal\ wall)\ or\ \partial T/\partial y = 0\ (adaibatic\ wall)$$

$$y\to\infty:\ u\to U_e,\ \ T\to T_e \tag{4}$$

In the previous equations, x and y are the distances measured along and perpendicular to the length of the plate and u and v are the velocity components in the corresponding directions. C_P is the specific heat; k the thermal conductivity; ρ the density; μ the viscosity; σ the electrical conductivity and B_0 is the magnetic field strength.

Proceeding with the analysis, we define the following transformations:

$$\xi=\rho_e U_e\mu_e\, x$$

$$\eta=\sqrt{\frac{\rho_e U_e}{2\mu_e x}}\int\frac{\rho}{\rho_e}\,dy$$

$$u=U_e f'(\eta)$$

$$T=T_e\, g(\eta) \tag{5}$$

Substituting the expressions in equation (5) into the governing equations (1) – (3) become

$$(C_1 f'')'+f f''+M\frac{\rho_e}{\rho}\left\{1-\left(\frac{\sigma}{\sigma_e}\right)f'\right\}=0 \tag{6}$$

$$(C_2 g')'+\frac{C_P}{C_{Pe}}Pr_e\ f\,g'+(\gamma_e-1)\,Ma_e^2\,Pr_e\,C_1\,(f'')^2=0 \tag{7}$$

where

$$C_1=\frac{\rho\,\mu}{\rho_e\mu_e}=\left(\frac{T}{T_e}\right)^{\frac{1}{2}}\left(\frac{T+c_m}{T_e+c_m}\right) \tag{8}$$

$$C_2=\frac{\rho\,k}{\rho_e k_e}=\left(\frac{T}{T_e}\right)^{\frac{1}{2}}\left(\frac{T+c_k}{T_e+c_k}\right) \tag{9}$$

$$c_m=110.4\,K \tag{10}$$

$$c_k = 194\,K \tag{11}$$

$$M = \frac{\sigma_e B_0^2}{\rho_e U_e} \tag{12}$$

Here c_m and c_k are chosen as in [6]

At high temperatures, the Oxygen and Nitrogen molecules are excited to the vibrational mode. The specific heat C_P may be written as

$$C_P = \frac{7}{2}\,R\,T + R\left(\frac{T_{ve}}{T}\right)^2 \frac{exp(T_{ve}/T)}{[exp(T_{ve}/T)-1]^2} \tag{13}$$

Here R represents gas constant and T_{ve} denotes the vibrational eigen temperature. We assume that $T_{ve} = 3030\,K$ (Liu and Cao [6]).

The transformed boundary conditions may be written as

$$f(0) = f_w,\;\; f\,'(0) = f_w',\;\; g(0) = \frac{T_w}{T_e} = g_w(isothermal\,wall);\; g'(0) = 0\;(adaibatic\;wall)$$

$$f\,'(\infty) = 1,\;\; g(\infty) = 1 \tag{14}$$

The local wall shear stress is given by

$$\tau_w = \mu\, \left.\frac{\partial u}{\partial y}\right)_{y=0} \tag{15}$$

We define

$$Re_x = \frac{\rho_e U_e\, x}{\mu_e}\;,\;\; C_{fx} = \frac{\tau_w}{\left(\frac{\rho\, U_e^2}{2}\right)} \tag{16}$$

The local friction factor may be written as

$$C_{fx} = \sqrt{2}\, Re_x^{-\frac{1}{2}}\, \frac{\mu_w}{\mu_e}\, f''(0) \tag{17}$$

For the isothermal wall case, the local heat flux can be written as

$$q_w = -k\, \left.\frac{\partial T}{\partial y}\right)_{y=0} - u_w\, \tau_w \tag{18}$$

In the previous equation, $q_w < 0$ indicates heat transferred to the surface. The local heat transfer coefficient is given by

$$h = \frac{q_w}{T_w - T_r} \tag{19}$$

The local Nusselt number becomes

$$Nu_x = -\frac{T_e}{(T_w - T_r)}\sqrt{\frac{Re_x}{2}}\,\frac{\rho_w}{\rho_e}\, g'(0) - \, Ec\,Pr\,\sqrt{\frac{Re_x}{2}}\,\frac{\rho_w}{\rho_e}\, f_w'\, f''(0) \tag{20}$$

where

$$Ec = \frac{U_e^2}{C_P(T_w - T_r)} \tag{21}$$

$$\frac{T_r}{T_e} = 1 + r\,\left(\frac{\gamma - 1}{2}\right) Ma^2 \tag{22}$$

3. RESULTS AND DISCUSSION

Equations (6) and (7) are solved numerically using the implicit finite difference method, Keller box method (Keller and Cebeci [9]).

3.1. Isothermal Wall Case

Tables **1-5** show the numerical results for wall shear stress $f''(0)$ and surface heat transfer $g'(0)$ with magnetic field M, Mach number Ma, surface mass transfer f_w, vectored surface mass transfer f_w' and surface temperature g_w are prescribable parameters.

Table 1: Effect of Magnetic Field M on $f''(0)$ and $-g'(0)$ for $Pr_e = 0.72,\; Ma = 5.0,\; f_w = 0.2,\; f_w' = 0.2,\; g_w = 4.0$ (Isothermal Wall Case)

M	$f''(0)$	$-g'(0)$
0	0.177076	0.024423
1	0.101768	0.291329
2	0.135422	0.299098
5	0.203162	0.309182
10	0.278869	0.306739

Table **1** shows that as the magnetic field parameter M increases, the wall shear stress and the surface heat transfer rate increase. The surface heat transfer rate increases by about tenfold when M increases from 0 to 10. This suggests that the magnetic force can be used to cool the surface at high Mach number applications.

Table 2: Effect of Mach Number Ma on $f''(0)$ and $-g'(0)$ for $Pr_e = 0.72,\; M = 5.0,\; f_w = 0.2,\; f_w' = 0.2,\; g_w = 4.0$ (Isothermal Wall Case)

Ma	$f''(0)$	$-g'(0)$
0.0	0.214943	0.543046
2.5	0.210750	0.465837
5.0	0.203162	0.309182
7.5	0.190139	-0.208486
10.0	-0.383989	-23.716007

Table **2** shows that as the Mach number parameter Ma increases, the wall shear stress and the surface heat transfer rate decrease. Positive values of $-g'(0)$ represent wall cooling and negative values for wall heating. Values of Ma above 5, corresponding to hypersonic speeds, produce wall heating instead of wall cooling. This is due to the intense viscous dissipation at high Mach numbers.

Table 3: Effect of Surface Mass Transfer f_w on $f''(0)$ and $-g'(0)$ for $Pr_e = 0.72$, $M = 5.0$, $Ma = 5.0$, $f'_w = 0.2$, $g_w = 4.0$ (Isothermal Wall Case)

f_w	$f''(0)$	$-g'(0)$
0.0	0.199932	0.270490
0.2	0.203162	0.309182
0.4	0.205839	0.341710
-0.2	0.196932	0.235632
-0.4	0.194037	0.201669

Table **3** indicates the wall shear stress and surface heat transfer rate increase due to increased momentum injection $(f_w > 0)$. Wall suction $(f_w < 0)$ produces reduced wall shear stress and heat transfer rate.

Table 4: Effect of Vectored Surface Mass Transfer f'_w on $f''(0)$ and $-g'(0)$ for $Pr_e = 0.72$, $M = 5.0$, $Ma = 5.0$, $f_w = 0.2$, $g_w = 4.0$ (Isothermal Wall Case)

f'_w	$f''(0)$	$-g'(0)$
0.0	0.927598	-0.629454
0.1	0.561263	-0.017278
0.2	0.203162	0.309182
0.3	-0.047972	1.024151
0.4	-0.415787	0.874210

Table **4** shows that the downstream vectored surface mass transfer reduces wall shear stress and heat transfer rates.

Table 5: Effect of Surface Temperature g_w on $f''(0)$ and $-g'(0)$ for $Pr_e = 0.72$, $M = 5.0$, $Ma = 5.0$, $f_w = 0.2$, $f'_w = 0.2$ (Isothermal Wall Case)

g_w	$f''(0)$	$-g'(0)$
2	0.895809	-0.836119
3	0.468507	0.016756
4	0.203162	0.309182
5	0.025295	0.588876
6	-0.066918	1.498548

Table **5** shows the effect of the value of surface temperature g_w on wall shear stress and heat transfer rate. As g_w increases, the wall shear stress decreases and heat transfer rate increases Figures **1** and **2** show the velocity and temperature distributions within the boundary layer for varying values of the magnetic field strength. As the value of M increases, both velocity and temperature decrease within the boundary layer.

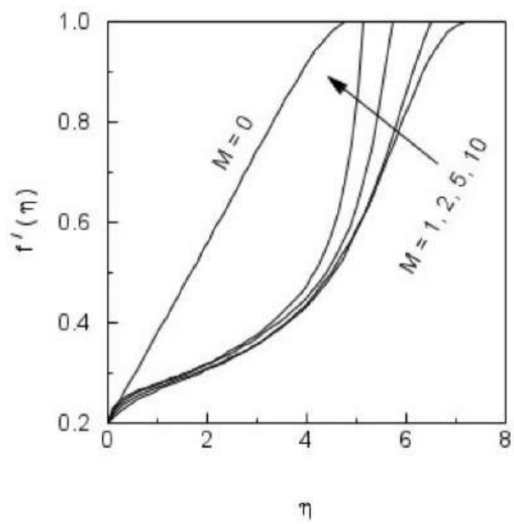

Figure 1: Effect of magnetic field M on $f'(\eta)$ for $Pr_e = 0.72$, $Ma = 5.0$, $f_w = 0.2$, $f'_w = 0.2$, $g_w = 4.0$ (Isothermal wall case).

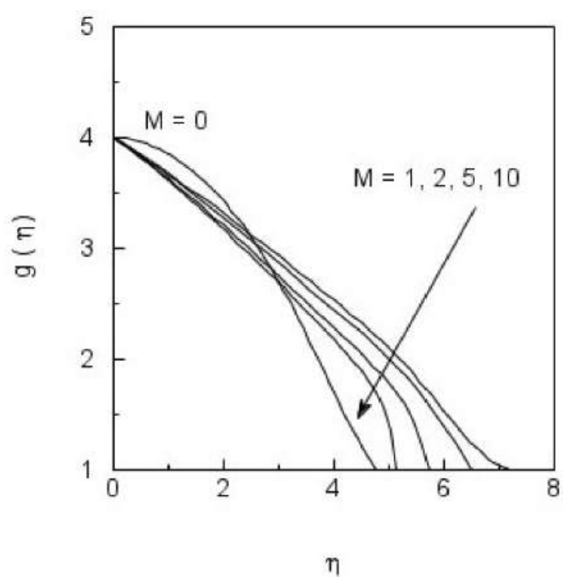

Figure 2: Effect of magnetic field M on $g(\eta)$ for $Pr_e = 0.72$, $Ma = 5.0$, $f_w = 0.2$, $f'_w = 0.2$, $g_w = 4.0$ (Isothermal wall case).

Figures **3** and **4** show the effect of Mach number Ma on the velocity and temperature distributions within the boundary layer. As the Mach number exceeds a value of 5, the boundary layer thickness becomes very small and the flow "wraps around" close to the surface.

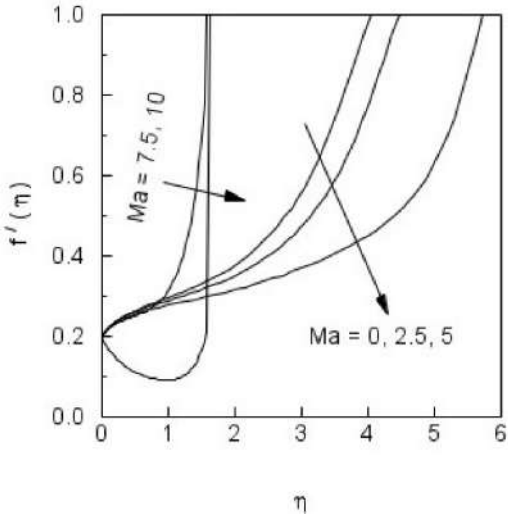

Figure 3: Effect of Mach number Ma on $f'(\eta)$ for $Pr_e = 0.72$, $M = 5.0$, $f_w = 0.2$, $f'_w = 0.2$, $g_w = 4.0$ (Isothermal wall case).

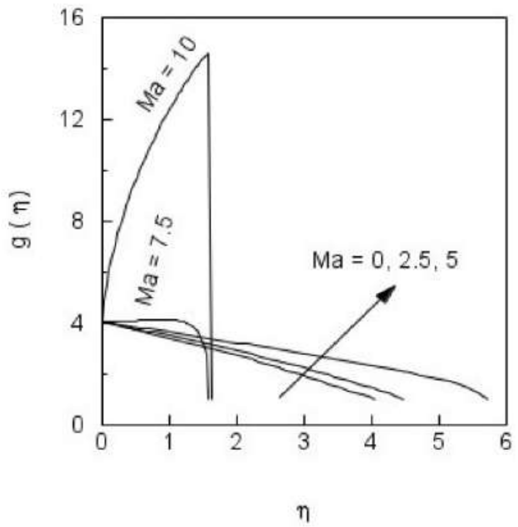

Figure 4: Effect of Mach number Ma on $g(\eta)$ for $Pr_e = 0.72$, $M = 5.0$, $f_w = 0.2$, $f'_w = 0.2$, $g_w = 4.0$ (Isothermal wall case).

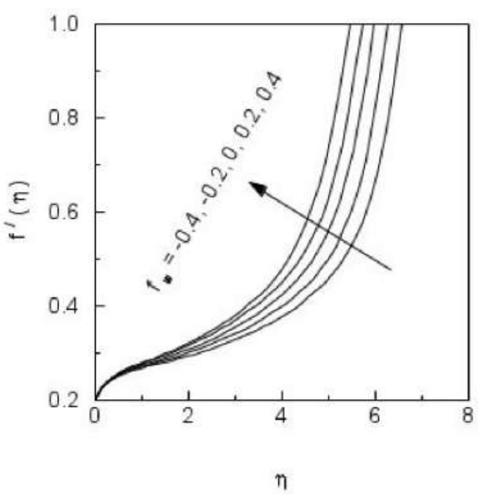

Figure 5: Effect of surface mass transfer f_w on $f'(\eta)$ for $Pr_e = 0.72$, $M = 5.0$, $Ma = 5.0$, $f'_w = 0.2$, $g_w = 4.0$ (Isothermal wall case).

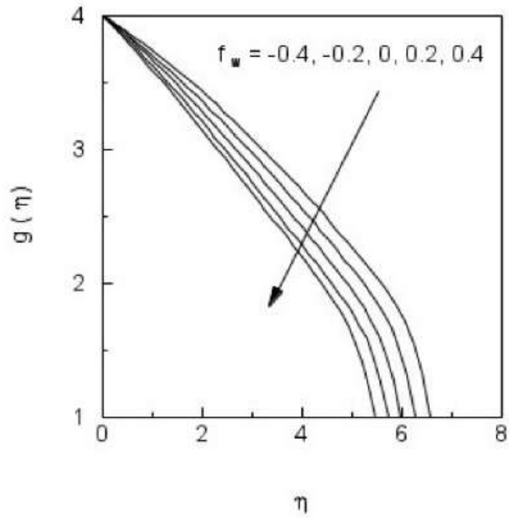

Figure 6: Effect of surface mass transfer f_w on $g(\eta)$ for $Pr_e = 0.72$, $M = 5.0$, $Ma = 5.0$, $f'_w = 0.2$, $g_w = 4.0$ (Isothermal wall case).

Figures **5** and **6** show that as $f_w$increases, the boundary layer thickness tends to reduce. The velocity at a distance normal to the surface increases whereas the temperature reduces.

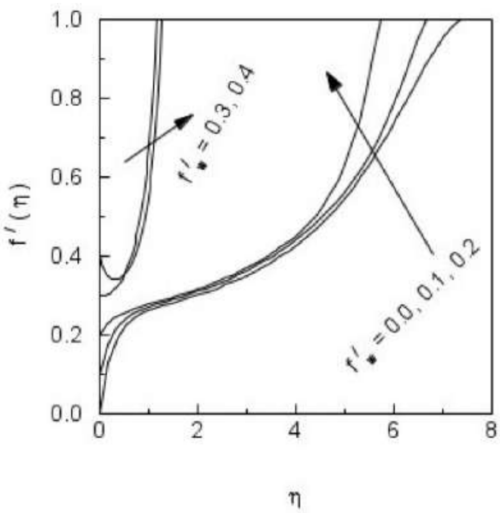

Figure 7: Effect of vectored surface mass transfer f'_w on $f'(\eta)$ for $Pr_e = 0.72$, $M = 5.0$, $Ma = 5.0$, $f_w = 0.2$, $g_w = 4.0$ (Isothermal wall case).

Figures **7** and **8** show that as f'_w increases, the boundary layer thickness tends to reduce. The velocity at a distance normal to the surface increases whereas the temperature reduces.

Figures **9** and **10** display result for the effect of wall temperature g_w on the velocity and temperature profiles. As g_w increases, the boundary layer thickness reduces. The velocity at a distance normal to the surface decreases whereas the temperature increases.

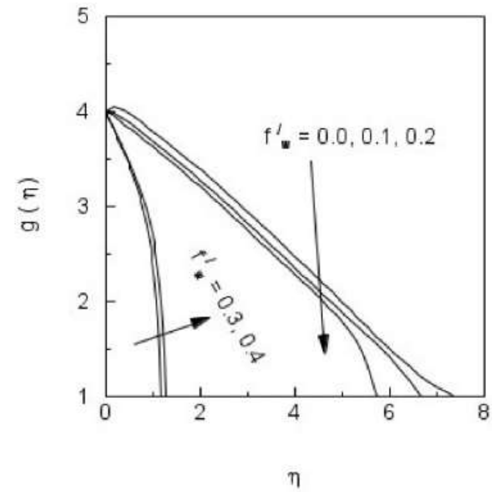

Figure 8: Effect of vectored surface mass transfer f_w' on $g(\eta)$ for $Pr_e = 0.72$, $M = 5.0$, $Ma = 5.0$, $f_w = 0.2$, $g_w = 4.0$ (Isothermal wall case).

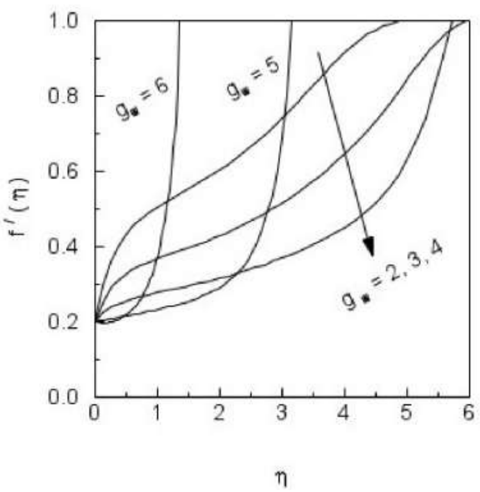

Figure 9: Effect of surface temperature g_w on $f'(\eta)$ for $Pr_e = 0.72$, $M = 5.0$, $Ma = 5.0$, $f_w = 0.2$, $f_w' = 0.2$ (Isothermal wall case).

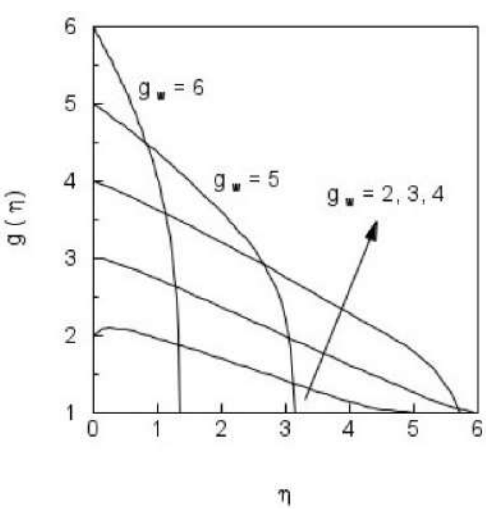

Figure 10: Effect of surface temperature g_w on $g(\eta)$ for $Pr_e = 0.72$, $M = 5.0$, $Ma = 5.0$, $f_w = 0.2$, $f_w' = 0.2$ (Isothermal wall case).

3.2. Adiabatic Wall Case

Tables **6-9** show the numerical results for wall shear stress $f''(0)$ and surface temperature $g(0)$ with magnetic field M, Mach number Ma, surface mass transfer f_w and vectored surface mass transfer f_w' are prescribable parameters.

Table 6: Effect of Magnetic Field M on $f''(0)$ and $g(0)$ for $Pr_e = 0.72$, $Ma = 2.5$, $f_w = 0.2$, $f_w' = 0.2$ (Adiabatic Wall Case)

M	$f''(0)$	$g(0)$
0.00	0.543364	1.623809
0.25	0.553556	1.653782
0.50	0.595215	1.676635
0.75	0.643863	1.692511
1.00	0.672274	1.713781
1.50	0.776507	1.723531
2.00	0.885384	1.722089
3.00	1.077941	1.717810
5.00	1.420840	1.705014

Table **6** shows that as the magnetic field parameter M increases, the wall shear stress and the surface temperature increase.

Table 7: Effect of Mach Number Ma on $f''(0)$ and $g(0)$ for $Pr_e = 0.72$, $M = 1$, $f_w = 0.2$, $f_w' = 0.2$ (Adiabatic Wall Case)

Ma	$f''(0)$	$g(0)$
1.0	1.219995	1.105356
1.5	0.953194	1.257377
2.0	0.794173	1.469765
2.5	0.672274	1.713781
3.0	0.629569	1.947499
4.0	0.594840	2.514951
5.0	0.618304	3.278970

Table **7** shows that as the Mach number parameter Ma increases, the wall shear stress decreases and the surface temperature increases. This is due to the intense viscous dissipation at high Mach numbers.

Table **8** indicates that wall blowing $(f_w > 0)$ results in increased wall shear stress and surface temperature. Wall suction $(f_w < 0)$ produces reduced wall shear stress and surface temperature.

Table 8: Effect of Surface Mass Transfer f_w on $f''(0)$ and $g(0)$ for $Pr_e = 0.72$, $M = 1$, $Ma = 2.5$, $f'_w = 0.2$ (Adiabatic Wall Case)

f_w	$f''(0)$	$g(0)$
0.0	0.637315	1.711502
0.2	0.672274	1.713781
0.4	0.709891	1.715896
-0.2	0.603583	1.709746
-0.4	0.583661	1.700628

Table 9: Effect of Vectored Surface Mass Transfer f'_w on $f''(0)$ and $g(0)$ for $Pr_e = 0.72$, $M = 1$, $Ma = 2.5$, $f_w = 0.2$ (Adiabatic Wall Case)

f'_w	$f''(0)$	$g(0)$
0.0	0.829564	2.117980
0.1	0.729355	1.912326
0.2	0.672274	1.713781
0.3	0.647298	1.533358
0.4	0.637642	1.379782

Table **9** shows that the downstream vectored surface mass transfer parameter f'_w reduces wall shear stress and surface temperature.

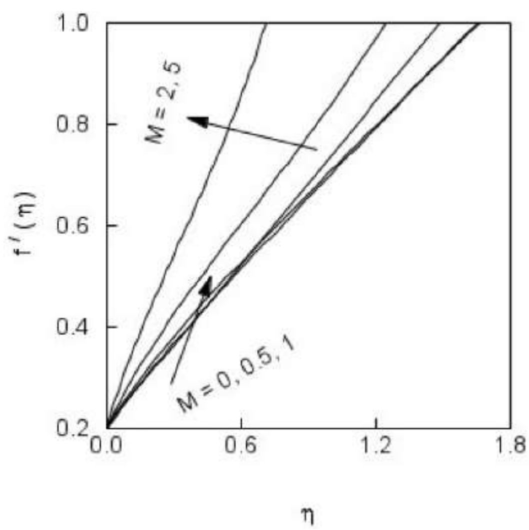

Figure 11: Effect of magnetic field M on $f'(\eta)$ for $Pr_e = 0.72$, $Ma = 2.5$, $f_w = 0.2$, $f'_w = 0.2$ (Adiabatic wall case).

Figures **11** and **12** show the velocity and temperature distributions within the boundary layer for varying values of the magnetic field parameter M strength. As the value of M increases, both velocity and temperature increase within the boundary layer.

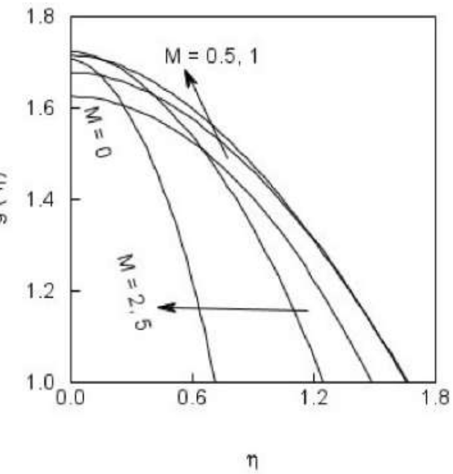

Figure 12: Effect of magnetic field M on $g(\eta)$ for $Pr_e = 0.72$, $Ma = 2.5$, $f_w = 0.2$, $f'_w = 0.2$ (Adiabatic wall case).

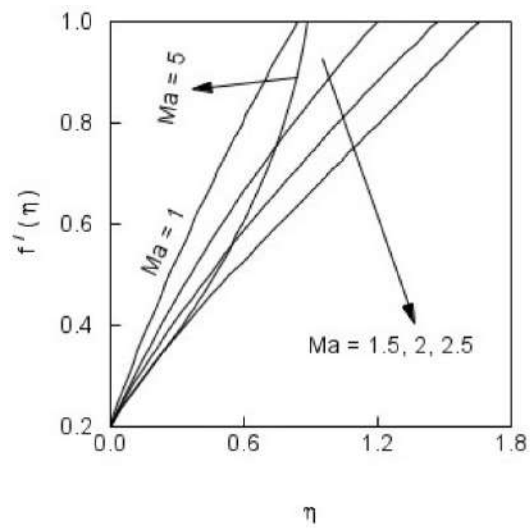

Figure 13: Effect of Mach number Ma on $f'(\eta)$ for $Pr_e = 0.72$, $M = 1$, $f_w = 0.2$, $f'_w = 0.2$ (Adiabatic wall case).

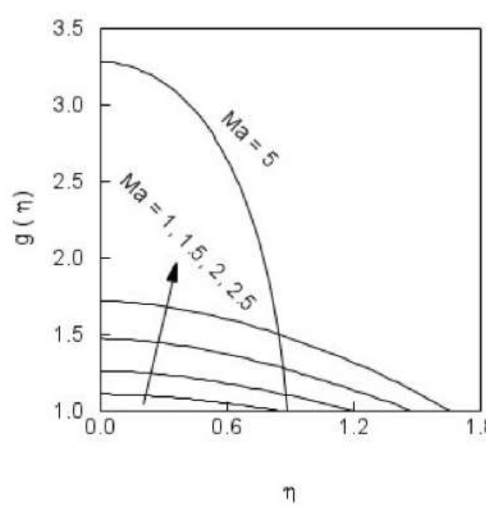

Figure 14: Effect of Mach number Ma on $g(\eta)$ for $Pr_e = 0.72$, $M = 1$, $f_w = 0.2$, $f'_w = 0.2$ (Adiabatic wall case).

Figures **13** and **14** show the effect of Mach Number parameter Ma on the velocity and temperature distributions within the boundary layer. As the Mach number exceeds a value of 5, the boundary layer thickness becomes very small and the flow "wraps around" close to the surface.

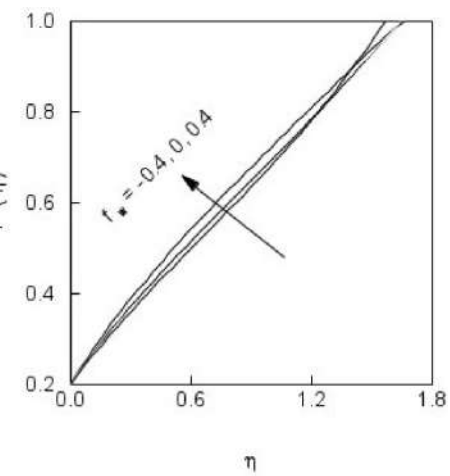

Figure 15: Effect of surface mass transfer f_w on $f'(\eta)$ for $Pr_e = 0.72$, $M = 1$, $Ma = 2.5$, $f_w' = 0.2$ (Adiabatic wall case).

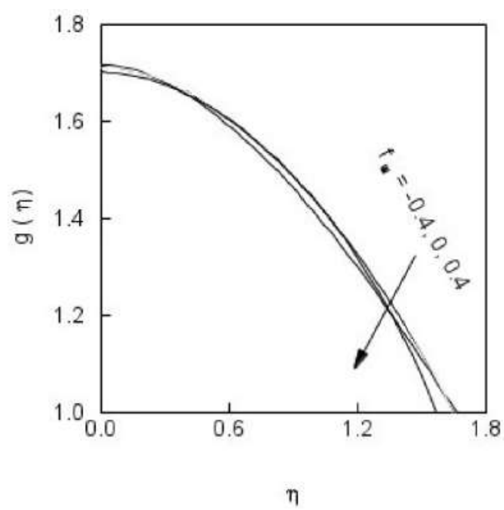

Figure 16: Effect of surface mass transfer f_w on $g(\eta)$ for $Pr_e = 0.72$, $M = 1$, $Ma = 2.5$, $f_w' = 0.2$ (Adiabatic wall case).

Figures **15** and **16** show that as surface mass transfer parameter f_w increases, the boundary layer thickness tends to reduce. The velocity at a distance normal to the surface increases whereas the temperature reduces.

Figures **17** and **18** show that as vectored surface mass transfer parameter f_w' increases, the boundary layer thickness tends to reduce. The velocity in the boundary layer increases and surface temperature decreases as f_w' increases.

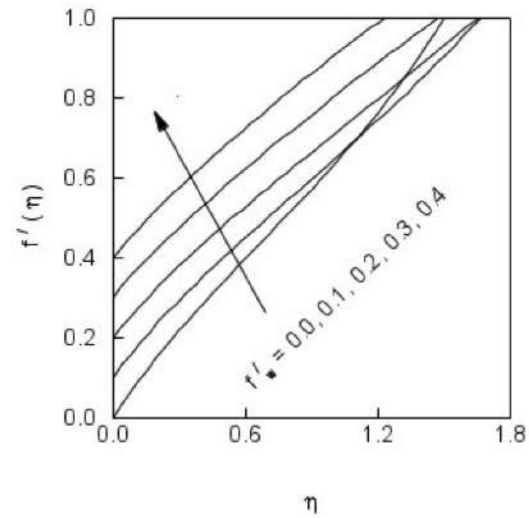

Figure 17: Effect of vectored surface mass transfer f_w' on $f'(\eta)$ for $Pr_e = 0.72$, $M = 1$, $Ma = 2.5$, $f_w = 0.2$ (Adiabatic wall case).

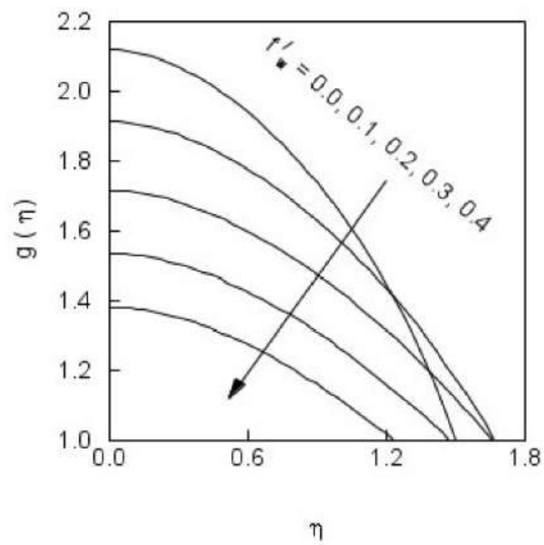

Figure 18: Effect of vectored surface mass transfer f_w' on $g(\eta)$ for $Pr_e = 0.72$, $M = 1$, $Ma = 2.5$, $f_w = 0.2$ (Adiabatic wall case).

4. CONCLUDING REMARKS

In this paper, a boundary layer analysis is presented for laminar, hypersonic flow over isothermal and adiabatic flat plates. Consideration is given to variable properties of air. It is shown that surface drag and heat transfer rates may be controlled by applying magnetic field and vectored surface mass transfer. The range of Mach numbers considered is 2.5 to 10. Increasing the magnetic field strength leads to higher friction factors and heat transfer rates, while vectored mass transfer effectively reduces both. Friction factor and surface temperature in the case of adiabatic surface can be reduced by applying vectored surface mass transfer.

ACKNOWLEDGEMENT

One of the authors (MK) is thankful to the Chairperson, Supercomputer Education and Research Centre, Indian Institute of Science, Bangalore, India, for providing computational facility.

NOTATION LIST

B_0 = Magnetic field strength

C_{fx} = local skin friction coefficient

C_p = specific heat

Ec = Eckert number

f = dimensionless stream function

f_w = dimensionless surface mass transfer parameter

f' = dimensionless velocity

f'_w = dimensionless vectored surface mass transfer parameter

$f''(0)$ = dimensionless wall shear stress

g = dimensionless temperature

g_w = dimensionless surface temperature parameter

$g(0)$ = dimensionless wall temperature

$g'(0)$ = dimensionless surface heat transfer

h = heat transfer coefficient

k = thermal conductivity

M = Magnetic field parameter (Hartmann number)

Ma = Mach number

Nu_x = Nusselt number

Pr = Prandtl number

q = heat flux

r = recovery factor

R = gas constant

Re_x = Reynolds number

T = temperature

T_{ve} = Vibrational eigen temperature

u = velocity component in streamwise direction

v = velocity component in normal direction

x = coordinate along streamwise direction

y = coordinate normal to the surface

γ = ratio of specific heats

η = dimensionless coordinate

μ = viscosity

ρ = density

Subscripts

e = conditions at the boundary layer edge

w = conditions at the wall

REFERENCES

[1] Tauber ME, Meneses GP. Aerothermodynamics of transatmospheric vehicles, AIAA 1986; AIAA Paper 86-1257. https://doi.org/10.2514/6.1986-1257

[2] Klopfer GH Yee HC. Viscous hypersonic shock-on-shock interaction on blunt cowl lips. AIAA 1988; AIAA Paper - 0233. https://doi.org/10.2514/6.1988-233

[3] Hoffmann KA, Siddiqui MS, Chang ST. Difficulties associated with the heat flux computations of high speed flows by the Navier-Stokes equations. AIAA 1991; AIAA Paper - 0467. https://doi.org/10.2514/6.1991-467

[4] Qu F, Sun D, Zuo G, Shi Y. An improvement on the AUSMPWM scheme for hypersonic heating predictions. International Journal of Heat and Mass Transfer 2017; 108: 2492-2501. https://doi.org/10.1016/j.ijheatmasstransfer.2016.12.031

[5] Zhang Z, Gao Z, Jiang C, Lee CH. A RANS model correctionon unphysical over-prediction of turbulent quantities across shock wave. International Journal of Heat and Mass Transfer 2017; 106: 1107-1119. https://doi.org/10.1016/j.ijheatmasstransfer.2016.10.087

[6] Liu C, Cao W. Study of predicting aerodynamic heating for hypersonic boundary layer flow over a flat plate. International Journal of Heat and Mass Transfer 2017; 111: 1079-1086. https://doi.org/10.1016/j.ijheatmasstransfer.2017.04.001

[7] Rossow VJ. On flow of electrical conducting fluids over a flat plate in the presence of a transverse magnetic field. NACA TN 3971, 1957.

[8] Gorla RSR. Heat transfer in wall jet flows with vectored surface mass transfer. AIAA Journal 1977; 15(10): 1514-1516. https://doi.org/10.2514/3.7447

[9] Keller HB Cebeci T. Accurate numerical methods for boundary layer flows 1. Two-dimensional flows. Proc. Int. Conf. Numerical Methods in Fluid Dynamics, Lecture Notes in Physics, Springer, New York 1971. https://doi.org/10.2514/6.1971-164